POLITECNICO DI TORINO
Repository ISTITUZIONALE

Micro-structured rough surfaces by laser etching for heat transfer enhancement on flush mounted heat sinks

Publisher copyright

(Article begins on next page)

04 August 2020

Micro-structured rough surfaces by laser etching for heat transfer enhancement on flush mounted heat sinks

Micro-structured rough surfaces by laser etching for heat transfer enhancement on flush mounted heat sinks

L Ventola[1], L Scaltrito[1,2], S Ferrero[1,2], G Maccioni[2], E Chiavazzo[1], P Asinari[1]

[1] multi-Scale ModeLing Laboratory (SMaLL), Energy Department, Politecnico di Torino, Corso Duca degli Abruzzi 24, 10129, Turin, Italy.
[2] Microla Optoelectronics S.r.l., Localita Baraggino 10034 Chivasso, Turin, Italy.

E-mail: `pietro.asinari@polito.it`

Abstract. The aim of this work is to improve heat transfer performances of flush mounted heat sinks used in electronic cooling. To do this we patterned 1.23 cm^2 heat sinks surfaces by micro-structured roughnesses built by laser etching manufacturing technique, and experimentally measured the convective heat transfer enhancements due to different patterns. Each roughness differs from the others with regards to the number and the size of the micro-fins (e.g. the micro-fin length ranges from 200 to 1100 μm). Experimental tests were carried out in forced air cooling regime. In particular fully turbulent flows (heating edge based Reynolds number ranging from 3000 to 17000) were explored. Convective heat transfer coefficient of the best micro-structured heat sink is found to be roughly two times compared to the smooth heat sinks one. In addition, surface area roughly doubles with regard to smooth heat sinks, due to the presence of micro-fins. Consequently, patterned heat sinks thermal transmittance [W/K] is found to be roughly four times the smooth heat sinks one. We hope this work may open the way for huge boost in the technology of electronic cooling by innovative manufacturing techniques.

1. Introduction

The heat fluxes electronic devices require to be dissipated continuously increase. The need of solutions able to deal with these high heat fluxes has led to explore a huge variety of methods and technologies. Liquid and two-phase based solutions have already been developed to properly cool down devices with high power density (e.g. high performance supercomputers). Nevertheless, forced air cooling techniques will remain the most suitable solutions in the foreseeable future for a large class of electronic devices, i.e. notebook and portable devices to name a few, because of their cheapness and reliability.

In the contest of air forced cooling regime, a variety of convective heat transfer enhancement techniques have been proposed in literature, such as plane fins [1, 2], pin fins [3, 4, 5], dimpled surfaces [6, 7, 8], surfaces with arrays of protrusions [9, 10], metal foams [11] and artificial surface roughness [12]. The term *artificial roughness* means any regular pattern build on the surface and purposely designed to enhance convective heat transfer. For instance, in such a category, we may include ribs [13, 14, 15] and, more recently, (shark-skin-like) scale roughened surfaces [16, 17]. The resulting heat transfer enhancement of the scale roughened surface is surprisingly

Table 1. Optimized laser parameters for copper processing.

Power [W]	frequency [kHz]	scan speed [mm/s]
7	10	100

good compared to rib roughened and dimpled surfaces [18]. The latter result proves that there is still room for improving the optimal design of artificial surface roughness. On the other hand innovative manufacturing techniques, e.g. additive manufacturing, are able to control process roughness of built surfaces. Recent works show the possibility to exploit the latter feature to produce flush mounted and finned heat sinks whose rough surfaces are able to enhance convective heat transfer[19].

In this work we focus on the possibility to enhance convective heat transfer of 1.23 cm^2 heat sinks surfaces patterned by artificial micro-structured roughnesses.

2. Laser etching manufacturing technique and samples characterization

In this paper, a novel technique, using nanoseconds DPSS laser direct writing on Copper substrate is studied. This class of laser is a flexible and effective tool characterized by low operating cost [20]. Laser radiation can be focused to micro-sized spots. A galvanometric head is used to control the laser beam position, thus a wide variety of low cost geometries can be obtained [21, 22]. Limited heat transport to minimize thermal degradation of the material outside the production zone is achieved by employing nanosecond pulse width. Short pulse widths, under the right conditions, can promote the spallation process that minimizes the volume of molten material produced and the subsequent no loss of geometry control because of its displacement. Moreover, the short pulse duration leads to high peak power, and therefore a very small heat-affected zone (HAZ) can be obtained.[23] Different lasers, such as picoseconds and femtoseconds allow a better control of the process, but the use of such classes of laser would increase dramatically the production costs, for instance the picoseconds and the femtoseconds laser can be up to five and ten times more cost intensive, respectively [24, 25]. On the contrary, nanosecond laser used in this study can be employed for a large scale of heat sinks production due to its low production costs. Besides, the nanoseconds laser are maintenance free at least up to three years per 24hr/7days working time.

We used laser etching manufacturing technique to build artificial micro-structured roughnesses on four copper samples. A DPPS laser system with emission at 532 nm has been employed. The laser parameters used for the machining are shown in Table1. Each sample is a cuboid of dimensions 11.1 mm x 11.1 mm x 5 mm, whom 11.1 mm x 11.1 mm surface has been manufactured in order to obtain a specific artificial roughness. Each roughness is made of micro-fins, namely cones or truncated cones, of uniform size arranged in staggered layout. Pictures of the samples are shown in Fig.1. Morphology of each samples has been characterized by a 3D optical scanner ATOS Compact Scan 2M (GOM GmbH). Field Emission Scanning Electron Microscope (FESEM) images of micro-fins built on each sample are shown in Fig.2. Geometrical parameters of tested samples are summarized in Table 2.

3. Experimental procedure

To measure the convective heat transfer coefficient a sensor purposely developed in a previous work[26] was used. This sensor is based on the key idea of using a thermal guard. A heater in the bottom of the sample generates a controlled heat flux. The sample is surrounded by a temperature controlled "guard" made of copper. This guard is kept at the same temperature of the sample, to force the heat to flows into the sample only. This ensures that the heat flux
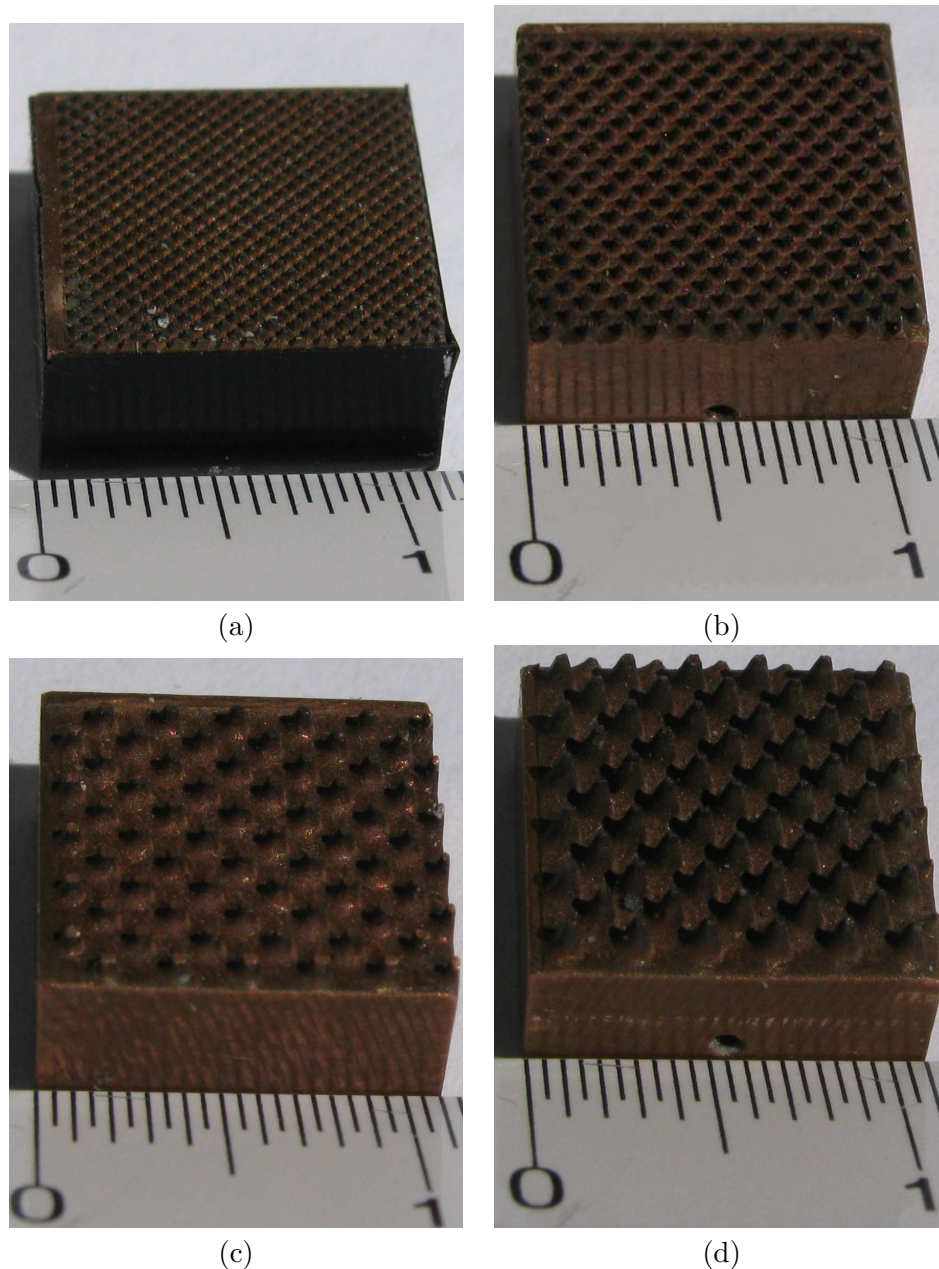
Figure 1. Picture of the four tested samples.

through the sample is essentially one-dimensional, going from the heater to the air flow passing through the sample itself. Temperature are measured by thermocouples in the sample and in the upstream and downstream (referring to fluid flow) part of the guard. The upstream and downstream part of the guard experience different values of convective heat transfer coefficient, due to leading edge effect. Hence, the guard will be slightly non isothermal, and some (undesired) temperature gradient between the sample and the guard (of the order of 0.2 K) could arise. For this reason a thermal insulating shield made of Teflon is placed between sample and guard. Its function is to minimize parasite conductive heat flux Q_k due to residual temperature gradients between sample and guard. In Fig 3 a view of the sensor is shown.
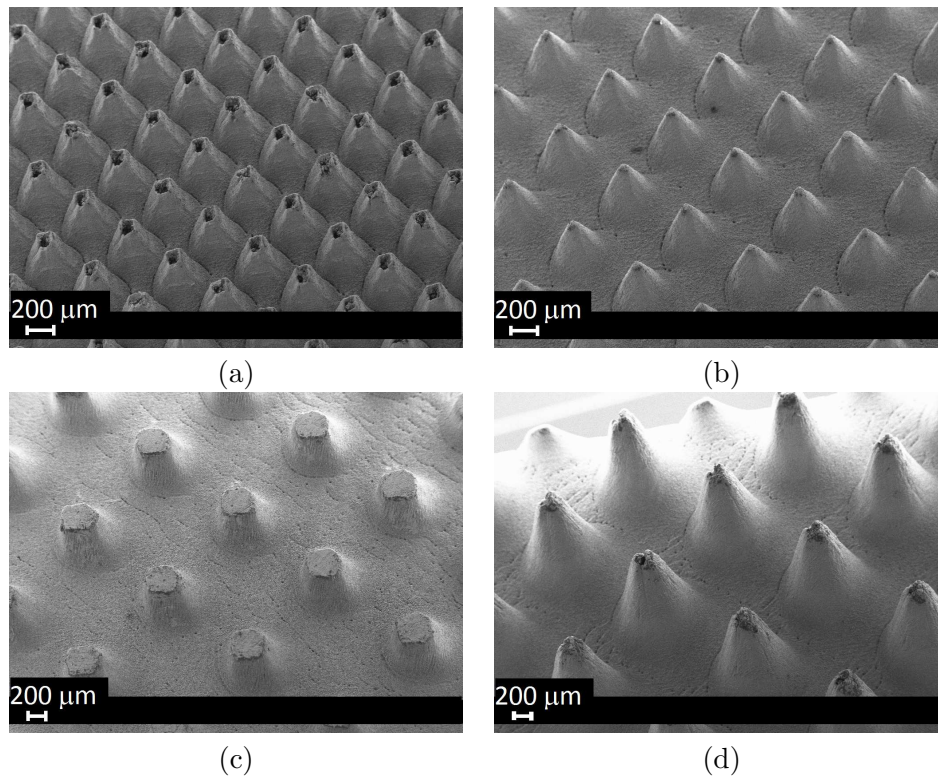
Figure 2. Morphological characterization of the four tested samples by Field Emission Scanning Electron Microscope (FESEM).

Table 2. Geometrical parameter of tested samples (see Fig.1): H, d_b, d_u, p and N are the average height, base diameter, upper diameter, distance (pinch) and number of micro-fins built on each sample, respectively (d_u is equal to 0 for cone-shaped fins and higher than 0 for truncated-cone-shaped fins, see Fig. 2). A is the sample surface area and $A_s = 123 \ mm^2$ is the smooth sample surface area.

Sample	H $[mm]$	d_b $[mm]$	d_u $[mm]$	p $[mm]$	N	A $[mm^2]$	A/A_s
(a)	0.20	0.48	0.00	0.49	465	154	1.25
(b)	0.35	0.52	0.00	0.65	253	185	1.50
(c)	0.65	0.85	0.35	1.35	72	177	1.44
(d)	1.10	1.00	0.00	1.35	61	240	1.95

The main portion of the power P provided by the heater to the sample is transferred into the air flow by convective heat transfer, while a minor, but far from negligible, portion of P is transferred to the wind channel walls through radiative heat transfer. Denoting by Q_c and Q_r the convective heat flux and the radiative heat flux respectively, we can calculate them by the following:

$$Q_r = \sigma_B \epsilon A (T_s^4 - T_w^4), \tag{1}$$

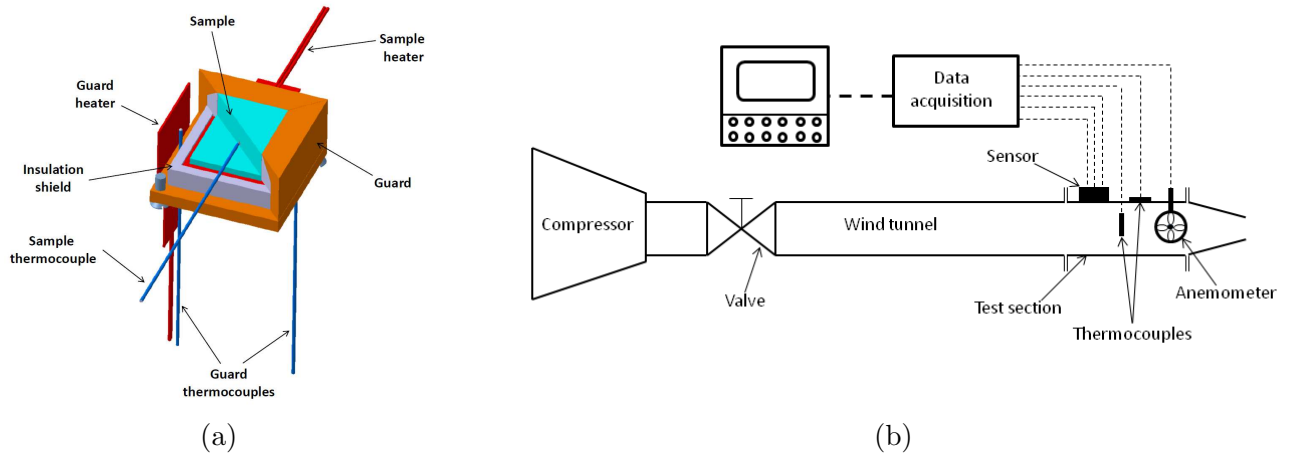$$Q_k = k[T_s - (T_{g1} + T_{g2})/2], \tag{2}$$

Figure 3. Isometric view of the convective heat transfer sensor (a), schematic diagram of the experimental facility (b) (see Ref. [26]).

$$Q_c = P - Q_r - Q_k = P - \sigma_B \epsilon A(T_s^4 - T_w^4) - k[T_s - (T_{g1} + T_{g2})/2], \tag{3}$$

where $\sigma_B = 5.67 \times 10^{-8} \, W/m^2/K^4$ is the Stefan-Boltzmann constant, $\epsilon = 0.23$ is the emissivity of the sample surface, T_s is the sample temperature measured by the thermocouple inserted in the center of the sample, T_w is the temperature of the channel wall, $k = 0.01 \, W/K$ is the sample-to-guard coupling conductive thermal transmittance [26], T_{g1} and T_{g2} are the temperatures measured by the (upstream and downstream) thermocouples installed into the thermal guard and A is the sample surface (see Table2). It is worth to note that Q_r and Q_k are less than 10% and 1% of P respectively, among all the tests. For each sample thermal transmittance Tr $[W/K]$ and convective heat transfer h $[W/m/K]$ can be calculated as:

$$Tr = \frac{Q_c}{T_s - T_a} = \frac{P - \sigma_B \epsilon A(T_s^4 - T_w^4) - k[T_s - (T_{g1} + T_{g2})/2]}{T_s - T_a}, \tag{4}$$

$$h = \frac{Q_c}{A(T_s - T_a)} = \frac{P - \sigma_B \epsilon A(T_s^4 - T_w^4) - k[T_s - (T_{g1} + T_{g2})/2]}{A(T_s - T_a)}, \tag{5}$$

where T_a is the air temperature.

The flow loop of the experimental system used in this work is the same used in previous works [19][26] and it is schematically shown in Fig. 3. An horizontal rectangular wind channel with cross section of $228 \, mm \times 158 \, mm$ (hydraulic diameter $187 \, mm$) and an entrance length of $5 \, m$ (corresponding roughly to 26 hydraulic diameters) is used. The air is blown by a Savio s.r.l. centrifugal fan type SFL 25-A, with a throttling valve for regulating the mass flow rate. At the end of the channel, downstream from the test section, a vane anemometer Testo 450 by Testo AG (sensitivity $\pm 0.1 \, m/s$) was used for measuring the axial velocity. The air temperature is measured at the same location where the anemometer is installed. Similarly, the channel wall temperature is measured by a thermocouple installed on the inner surface of the channel. Chromel-Alumel (type K) thermocouples were used for all temperature measurements. Two PS3003 variable power suppliers are used to feed both the sample and the guard heater. Finally, a six-digits, electronic multimeter (Agilent 34401A) is used to measure the voltage to the sample heater.

4. Results

Convective heat transfer coefficient h $[W/m^2/K]$ and thermal transmittance Tr $[W/K]$ of each sample have been measured for different velocities, in order to investigate the heat transfer phenomenon in a wide range of fluid flows. In addition h and Tr have been measured also for a smooth (without micro-fins) surface sample, obtained by traditional milling.

To each value of mean velocity u inside the wind tunnel we associated the dimensionless Reynolds number Re_L, calculated according to the formula:

$$Re_L = uL/\nu \tag{6}$$

with $\nu = 1.493\ 10^{-5}\ m^2/s$ being kinematic viscosity of air and $L = 20\ mm$ being the characteristic heated edge, namely the guard. Conversely, the average convective heat transfer coefficient h was expressed in terms of dimensionless number $Nu/Pr^{\frac{1}{3}}$, whereas:

$$Nu = hL/k \tag{7}$$

is the dimensionless Nusselt number and

$$Pr = \nu/\alpha \tag{8}$$

is the dimensionless Prandtl number with $\alpha = 2.224\ 10^{-5}\ m^2/s$ and $k = 2.83\ 10^{-2}\ W/m/K$ being the thermal diffusivity and thermal conductivity of air respectively.

It is worth to note that temperature gradient along the micro-fins length is negligible among all the samples, i.e. fin efficiency of micro-fins could be considered 100% among all the samples. To prove the latter claim we calculated the dimensionless fin parameter mL for each conical fin, where L is the fin height H defined in table 2, and m is defined as:

$$m = (\frac{4h_{max}}{k_{Cu}d_b})^{0.5} \tag{9}$$

where $k_{Cu} = 390\ W/m/K$ is the thermal conductivity of copper, and h_{max} is the maximum convective heat transfer coefficient experimentally measured. the mL parameter is less then 0.05 for all the fin configurations, consequently fin efficiency of micro-fins could be considered 100% among all the samples according [27].

In Fig.4 the experimental results in term of thermal transmittance Tr $[W/K]$ as a function of Reynolds number Re_L are shown. It could be noticed in Fig.4 that micro-structured sample (d) achieve in the high Reynolds number regime a thermal transmittance which is roughly four times the reference smooth sample one. In addition we note that, in the air velocity range under consideration in this study, samples with higher micro-fin height H (see table 2) are characterized by higher thermal transmittance than the other samples. This is due to two main reasons: The first is that height of the fins strongly affects the fluid dynamics interactions between the flow field and the fins themselves, and consequently the convective heat transfer phenomena. The second is that, due to peculiar geometrical dimensions of the samples under consideration in this study, higher fins belong to samples with higher surface area, except for sample (c) which has higher fins but a slightly lower surface area than sample (b) (see table 2). Obviously samples with higher surface area available for convective heat transfer are supposed to have higher thermal transmittance Tr than the other samples.

In order to split the contribution of the increase in surface area and of fluid dynamic interactions on heat transfer enhancement, it is worth to analyze the dimensionless Nusselt number Nu_L. This quantity allow us to remove the contribution of the increase in surface area on heat transfer enhancement, and consequently to study the portion of heat transfer enhancement due to fluid dynamics interactions only. In Fig.5 the experimental results in term
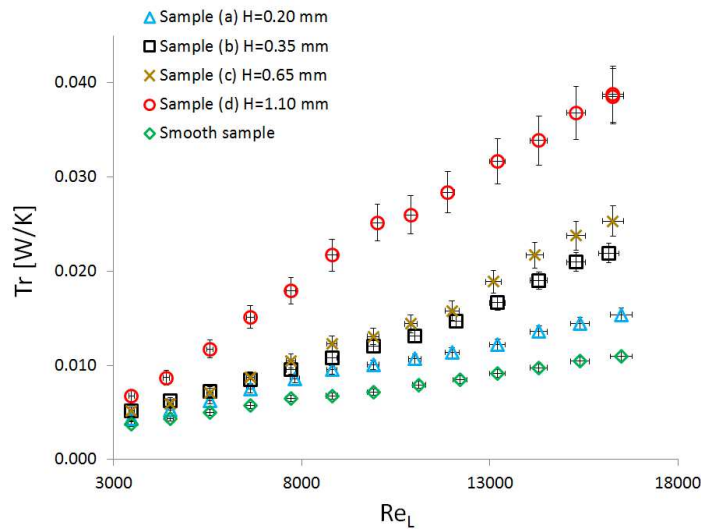
Figure 4. Experimental results for micro-structured artificial rough samples and reference smooth sample, Tr versus Re_L.
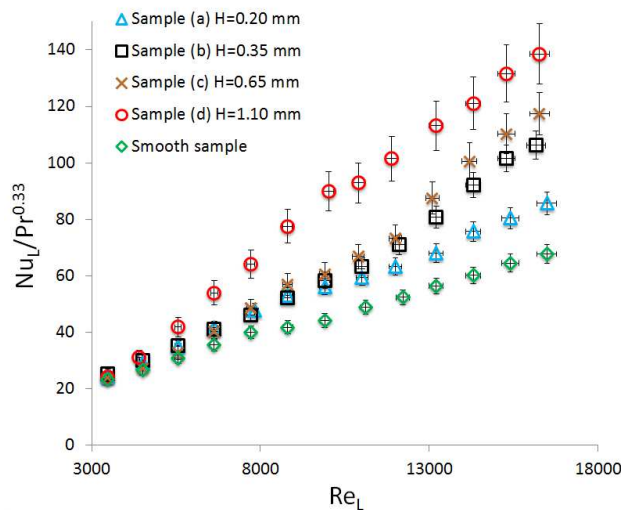

Figure 5. Experimental results for micro-structured artificial rough samples and reference smooth sample, Nu_L versus Re_L.

of Nusselt number Nu_L as a function of Reynolds number Re_L are shown. It could be noticed that micro-structured sample (d) achieve in the high Reynolds number regime a Nu_L value which is roughly two times the reference smooth sample one. In addition we note that, in the air velocity range under consideration in this study, samples with higher micro-fin height H (see table 2) are characterized by higher value of Nu_L than the other samples. The reason behind this phenomenon could be found analyzing the near-wall velocity profile.

The pressure gradient inside a pipe can be expressed as a function of the dimensionless friction factor f, namely $\nabla p = (f/D) \rho v^2/2$. In case of smooth pipe turbulent flow, the friction factor can expressed by the phenomenological correlation proposed by Blasius [28],

$f_B = f_B(Re_D) = 0.3164 \, Re_D^{-1/4}$, where Re_D is the Reynolds number based on the pipe diameter and on the average flow speed. The shear stress at the wall of a pipe τ is related to the pressure gradient inside the pipe ∇p by the linear relation $\tau = \nabla p \, D/4$, where D is the pipe diameter. Combining the previous relations yields $\tau = (f/8) \, \rho \, v^2/2$. The shear stress can be used to define the friction velocity v_*, namely $v_* = \sqrt{\tau/\rho} = v \, \sqrt{f/8}$, and, consequently, the friction length $y_0 = \nu/v_*$, where ν is the kinematic viscosity of the fluid. The friction length y_0 is useful to define a dimensionless distance from the wall, $y^+ = y/y_0$ (with y being the distance from the wall) and to formulate the following logarithmic law due to Von Kármán, $v^+ = v/v_* = \kappa^{-1} \ln y^+ + A$, where κ is the Von Kármán's constant and A is a constant for smooth walls. The friction length can be expressed as

$$y_0 = \frac{D}{Re_D \, \sqrt{f_B/8}}, \tag{10}$$

where

$$Re_D = uD/\nu \tag{11}$$

is the Reynolds number based on the wind channel hydraulic diameter $D = 0.187 \, m$. In our experiments Re_D and y_0 lay in the ranges $[3 \, 10^4 \div 1.6 \, 10^5]$ and $[0.026 \div 0.11 \, mm]$, respectively. Consequently, even in case of the highest Reynolds number $Re_D = 1.6 \, 10^5$, i.e. thinnest boundary layer ($y_0 = 0.026 \, mm$), we find $H/y_0 < 45$ among all the tested samples. That means micro-fins of all the tested samples lies in the buffer layer region or in the early log-law region [29], depending on the sample tested, i.e. fin height H, and on the flow field conditions, i.e. value of y_0. Hence fins lies in a portion of the boundary layer in which the velocity is still very sensitive to the distance from the wall, namely the fin root surface. Consequently we can argue higher fins experience an higher heat transfer because they are flushed by a stronger flow field than the shorter ones.

On the other hand, it could be noticed in Fig. 5 that in the low Reynolds number region there is a superposition of experimental points belonging to different samples. Also in this case we can provide an explanation of the phenomenon analyzing the nature of the near wall flow field. Data in Fig. 5 show different samples experience the same curve $Nu_L = f(Re_L)$ if the corresponding fin height is less than $l = 12y_0$, namely roughly two times the viscous sub layer thickness $y_{VSL} = 5y_0$. In particular $y_0 = 0.093mm$ for very low Reynolds number, i.e. $Re_D = 3.7 \, 10^4$ corresponding to $Re_L = 4 \, 10^3$, (see Eq.10) leading to $l = 1.1mm$ which is exactly the size of the higher fin height (see Tab.2, sample (d)). Consequently all the samples experience the same value of Nu_L for $Re_L \leq 4 \, 10^3$. As Reynolds number increase, y_0 decrease (i.e. thinner boundary layer), leading size of fin height of sample (d) to exceed the threshold level $l = 12y_0$ and consequently to experience higher values of Nu_L than the other samples. For $Re_D = 7.5$ 10^4 corresponding to $Re_L = 8 \, 10^3$, $y_0 = 0.054mm$ leading to $l = 0.65mm$ which is exactly the fin height of sample (c). As shown in Fig.5 for $Re_L \leq 8 \, 10^3$ all finned samples but sample (d) experience the same curve $Nu_L = f(Re_L)$. On the contrary, when Reynolds number increase further each sample experience a different trend, due to the different sample geometrical features an consequently to the different nature of interactions between the fluid flow and the fin walls, as discussed above.

Uncertainty values shown in Figs.4, 5 have been calculated with regard to a significant level $\alpha = 0.05$ (5 %). Both type A and type B uncertainties have been considered. Concerning type B uncertainties, Eqs. (4, 5) allows one to compute Tr and h respectively, as a function of other measurements $(P, T_s, T_{g1}, T_{g2}, T_a, T_w, \epsilon)$. These independent quantities can be organized in a vector, namely $\boldsymbol{q} := \{P, T_s, T_{g1}, T_{g2}, T_a, T_w, \epsilon\}$, and $q_i \in \boldsymbol{q}$ is the generic i-th quantity. The

standard uncertainty $\Sigma_{h,B}$ can be computed by the uncertainty estimation method [30] as

$$\Sigma_{h,B} = \sqrt{\sum_{i=1}^{7}\left(\Sigma_{q_i}\frac{\partial h}{\partial q_i}\right)^2}, \tag{12}$$

where Σ_{q_i} is the standard uncertainty for the quantity q_i, reported in [26], Table 1. On the other hand, type A uncertainties have been calculated using both t-student and chi-squared distributions by mean of a novel method proposed in [26]. Combining type A and type B uncertainties [26] is possible to calculate the overall uncertainty values, as shown in Figs.4, 5. It is worth to highlight that the previous procedure allows one to compute tolerance intervals, which are wider than confidence intervals and more robust estimates of the experimental uncertainty. The maximum and mean relative uncertainty for the convective heat transfer coefficient is $\pm 9.4\%$ and $\pm 6.4\%$, respectively.

5. Conclusions

In this work heat transfer performances of forced air cooled flush mounted heat sinks have been improved by pattering heat sinks surfaces with micro-structured artificial roughnesses obtained by laser etching manufacturing technique. Each structured roughness is made of micro-metric structures, namely truncated cones, of uniform size arranged in staggered layout. In particular each sample differs from the others with regards to the number and the size of the micro-fins (e.g. the micro-fin length ranges from 200 to 1100 μm). Experimental tests were carried out in forced air cooling regime. In particular fully turbulent flows (heating edge based Reynolds number ranging from 3000 to 17000) have been explored. Convective heat transfer coefficient of the best micro-structured heat sink is found to be roughly two times compared to the smooth heat sinks one. In addition, surface area roughly doubles with regard to smooth heat sinks, due to the presence of micro-fins. Consequently, patterned heat sinks thermal transmittance [W/K] is found to be roughly four times the smooth heat sinks one. An effective physical interpretation of the enhancement and of its dependency on the air velocity is provided in this work. In particular, the dependency of the enhancement on both geometrical and fluid dynamics characteristic length scales is demonstrated. In particular this study demonstrate that micro-fin whose height lays between the buffer layer and the early log-law region, i.e. $30 \leq y_0 \leq 45$, can lead to a huge enhancement in thermal transmittance due to interactions between the fluid flow and the fin walls, besides the augmentation in surface area available for heat transfer. The enhancement in thermal transmittance due to fluid-wall interaction has been proven to be effective when micro-fin height exceed $12y_0$, i.e. roughly two times the viscous sub layer thickness, for the samples under consideration. For this reason, this works provides preliminary guidelines to the design of micro-structured artificial rough surface for enhanced heat transfer.

Beyond laser etching, there are other interesting techniques to realize micro-structured rough geometries, e.g. additive manufacturing [19]. As an outlook, based on the present results, we plan further studies focusing on investigation and optimization of micro-structured surfaces and design of hierarchical solutions able to coupling micro- and macro- structures.

References
[1] J.R. Culham, Y.S. Muzychka, Optimization of plate fin heat sinks using entropy generation minimization, IEEE Transactions on Components and Packaging Technologies 24:2 (2001) 159-165.

[2] C.J. Shih, G.C. Liu, Optimal design methodology of plate-fin heat sinks for electronic cooling using entropy generation strategy, IEEE Transactions on Components and Packaging Technologies 27:3 (2004) 551-559.

[3] W.A. Khan, J.R. Culham, M.M. Yovanovich, The Role of Fin Geometry in Heat Sink Performance, Journal of Electronic Packaging 128:4 (2006) 324-330.

[4] S.W. Chang, T.L. Yang, C.C. Huang, K.F. Chiang, Endwall heat transfer and pressure drop in rectangular channels with attached and detached circular pin-fin array, International Journal of Heat and Mass Transfer 51:21-22 (2008) 5247-5259.

[5] Y.-T. Yang, H.-S. Peng, Numerical study of pin-fin heat sink with un-uniform fin height design, International Journal of Heat and Mass Transfer 51:19-20 (2008) 4788-4796.

[6] P.M. Ligrani, G.I. Mahmood, J.L. Harrison, C.M. Clayton, D.L. Nelson, Flow structure and local Nusselt number variations in a channel with dimples and protrusions on opposite walls, International Journal of Heat and Mass Transfer 44:23 (2001) 4413-4425.

[7] M.A. Elyyan, A. Rozati, D.K. Tafti, Investigation of dimpled fins for heat transfer enhancement in compact heat exchangers, International Journal of Heat and Mass Transfer 51:11-12 (2008) 2950-2966.

[8] Y. Chen, Y.T. Chew, B.C. Khoo, Enhancement of heat transfer in turbulent channel flow over dimpled surface, International Journal of Heat and Mass Transfer 55:25-26 (2012) 8100-8121.

[9] S.V. Garimella and P.A. Eibeck, Heat transfer characteristics of an array of protruding elements in single phase forced convection, Internal Journal of Heat and Mass Transfer 33:12 (1990) 2659-2669.

[10] G.I. Mahmood, M.Z. Sabbagh, P.M. Ligrani, Heat Transfer in a Channel with Dimples and Protrusions on Opposite Walls, Journal of Thermophysics and Heat Transfer 15:3 (2001) 275-283.

[11] S. Mancin, C. Zilio, A. Diani, L. Rossetto, Air forced convection through metal foams: Experimental results and modeling, International Journal of Heat and Mass Transfer 62:1 (2013) 112-123.

[12] E.K. Kalinin, G.A. Dreitser, Heat Transfer Enhancement in Heat Exchangers, Advances in Heat Transfer 31:C (1998) 159-332.

[13] J.S. Park, J.C. Han, Y. Huang, S. Ou, R.J. Boyle, Heat transfer performance comparisons of five different rectangular channels with parallel angled ribs, International Journal of Heat and Mass Transfer 35:11 (1992) 2891-2903.

[14] X. Gao, B. Sunden, Heat transfer and pressure drop measurements in rib-roughened rectangular ducts, Experimental Thermal and Fluid Science 24:1-2 (2001) 25-34.

[15] G. Tanda, Heat transfer in rectangular channels with transverse and V-shaped broken ribs, International Journal of Heat and Mass Transfer 47:2 (2004) 229-243.

[16] S.W. Chang, T.-M. Liou, M.H. Lu, Heat transfer of rectangular narrow channel with two opposite scale roughened walls, International Journal of Heat and Mass Transfer 48:19-20 (2005) 3921-3931.

[17] S.W. Chang, T.M. Liou, K.F. Chiang, G.F. Hong, Heat transfer and pressure drop in rectangular channel with compound roughness of V-shaped ribs and deepened scales, International Journal of Heat and Mass Transfer 51:3-4 (2008) 457-468.

[18] F. Zhou, G.W. Demoulin, D.J. Geb, I. Catton, Closure for a plane fin heat sink with scale-roughened surfaces for volume averaging theory (VAT) based modeling, International Journal of Heat and Mass Transfer 55:25-26 (2012) 7677-7685.

[19] L. Ventola, F. Robotti, M. Dialameh, F. Calignano, D. Manfredi, E. Chiavazzo and P. Asinari, Rough surfaces with enhanced heat transfer for electronics cooling by direct metal laser sintering, International Journal of Heat and Mass Transfer 75 (2014) 5874.

[20] M. Mullenborn, H. Dirac, J. Petersen, S. Bouwstra, Fast three dimensional laser micromachining of silicon for microsystem, Sensors and Actuators 52 (1996) 121-125.

[21] J. Chang, B. Warner, E. Dragon, M. Martinez, Precision micromachining with pulsed green laser, J. Laser Appl. 10:6 (1998) 285-290.

[22] M.R.H. Knowles, G. Rutterford, A.I. Bell, A.J. Andrews, G. Foster-Turner, A.J. Kearsley, Sub-micron and high precision micromachining using nanosecond lasers, Proceedings of ICALEO 112-120 (1998).

[23] T. Otani, L. Herbst, M. Heglin, S.V. Govorkov, A.O. Wiessner, Microdrilling and micromachining with diode-pumped solid state laser, Appl. Phys. 79 (2004) 1335-1339.

[24] www.rofin.it/

[25] www.lightcon.com/

[26] E. Chiavazzo, L. Ventola, F. Calignano, D. Manfredi, P. Asinari, A sensor for direct measurement of small convective heat fluxes: Validation and application to micro-structured surfaces, Experimental Thermal and Fluid Science 55 (2014) 42-53.

[27] A. Bejan and A.D. Kraus (Editors), Heat Transfer Handbook, John Wiley, Hoboken (2003).

[28] H. Schlichting, K. Gersten, Boundary-layer theory, Springer, 8th ed., Berlin, 2000.

[29] S.B. Pope, Turbulent Flows, Cambridge University Press, 2000.

[30] J. Mandel, The Statistical Analysis of Experimental Data, Dover, New York, (1984).